REPORT DOCUMENTATION PAGE

Form Approved
OMB No. 0704-0188

1. AGENCY USE ONLY (Leave blank)	2. REPORT DATE	3. REPORT TYPE AND DATES COVERED
	December 28, 1989	

4. TITLE AND SUBTITLE

Angle Estimation in the Presence of Mainbeam Interference

5. FUNDING NUMBERS

PE - 63319N
TA - R1973
WU - DN156-470

6. AUTHOR(S)

Lin, F. C. and Kretschmer, F. F., Jr.

7. PERFORMING ORGANIZATION NAME(S) AND ADDRESS(ES)

Naval Research Laboratory
Washington, DC 20375-5000

8. PERFORMING ORGANIZATION REPORT NUMBER

NRL Report 9234

9. SPONSORING/MONITORING AGENCY NAME(S) AND ADDRESS(ES)

Naval Sea Systems Command
Washington, DC 20362-5101

10. SPONSORING/MONITORING AGENCY REPORT NUMBER

11. SUPPLEMENTARY NOTES

12a. DISTRIBUTION/AVAILABILITY STATEMENT

Approved for public release; distribution unlimited.

12b. DISTRIBUTION CODE

13. ABSTRACT *(Maximum 200 words)*

Angle of arrival of a desired signal in a mainbeam interference environment can be estimated by incorporating adaptive array processing. Adapted sum and difference beams that suppress the undesired noise sources are used to determine the monopulse error curve. The resultant distorted error curve across the mainbeam tracking angle region is used directly for angle estimation. The Cramer-Rao bound on the angle estimation error is derived with generalized assumptions on the signal characteristics. A Monte Carlo simulation is performed for the estimation procedure described here, and the angle estimation error is then compared with the Cramer-Rao bound. It is shown that good performance in angle measurement can be achieved with sufficient signal-to-noise ratio and angular separation between the target and the interference sources.

14. SUBJECT TERMS

Angle estimation
Adaptive arrays
Cramer-Rao bound
Mainbeam interference
Monopulse tracking

15. NUMBER OF PAGES

27

16. PRICE CODE

17. SECURITY CLASSIFICATION OF REPORT	18. SECURITY CLASSIFICATION OF THIS PAGE	19. SECURITY CLASSIFICATION OF ABSTRACT	20. LIMITATION OF ABSTRACT
UNCLASSIFIED	UNCLASSIFIED	UNCLASSIFIED	

Naval Research Laboratory
Washington, DC 20375-5000

NRL Report 9234

Angle Estimation in the Presence of Mainbeam Interference

by

FENG-LING C. LIN AND FRANK F. KRETSCHMER, JR.

Target Characteristics Branch
Radar Division

December ~~28,~~ 1989

CONTENTS

ANGLE ESTIMATION IN THE PRESENCE OF MAINBEAM INTERFERENCE

I. INTRODUCTION

The problem of target tracking in the presence of mainbeam interference is of considerable interest in radar systems. Conventional tracking radars may experience serious errors in this situation. This problem was first addressed in the literature by Davis et al. [1], who extended the theory of adaptive arrays to the angle measurement problem based on maximum likelihood theory. They proposed an angle-of-arrival estimator involving adaptively distorted sum and difference beams that are analogous to those used in conventional monopulse antennas. Good performance by simulation was demonstrated for sidelobe and mainbeam interference.

The approach taken by Gabriel [2] was to determine the monopulse error curve from the adapted sum and difference beams in which the interference signals have been suppressed. The resultant distorted error curve across the mainbeam tracking angle region was used directly for track correction. This approach can be easily implemented and is used here to estimate the angle of arrival in the presence of both internal noise and external interference sources located within the mainbeam of the array antenna. Monte Carlo simulation is performed to evaluate the approach, and the angle estimation errors are obtained. These errors are compared with the Cramer-Rao bound, which provides the minimum error for an unbiased estimator. This bound is derived for the general case consisting of unknown signal amplitude, phase, and angle of arrival. The bound has been previously derived by others [3,4] but under different conditions.

II. PROBLEM FORMULATION

The received baseband complex signal X_k at the kth element of an N-element antenna array, as illustrated in Fig. 1, is given by

$$X_k = S\, e^{j(2\pi/\lambda)(k-1)d \sin\phi_S} + \sum_{i=1}^{N_J} r_i e^{j(2\pi/\lambda)(k-1)d \sin\psi_i} + n_k, \tag{1}$$

where

S is the complex target echo,
ϕ_S is the angle of arrival of the target,
r_i is the complex signal of the ith interference source,
ψ_i is the angle of arrival of the ith interference source,
N_J is the total number of interference sources,
n_k is the thermal noise at the kth element,

Manuscript approved August 4, 1989.

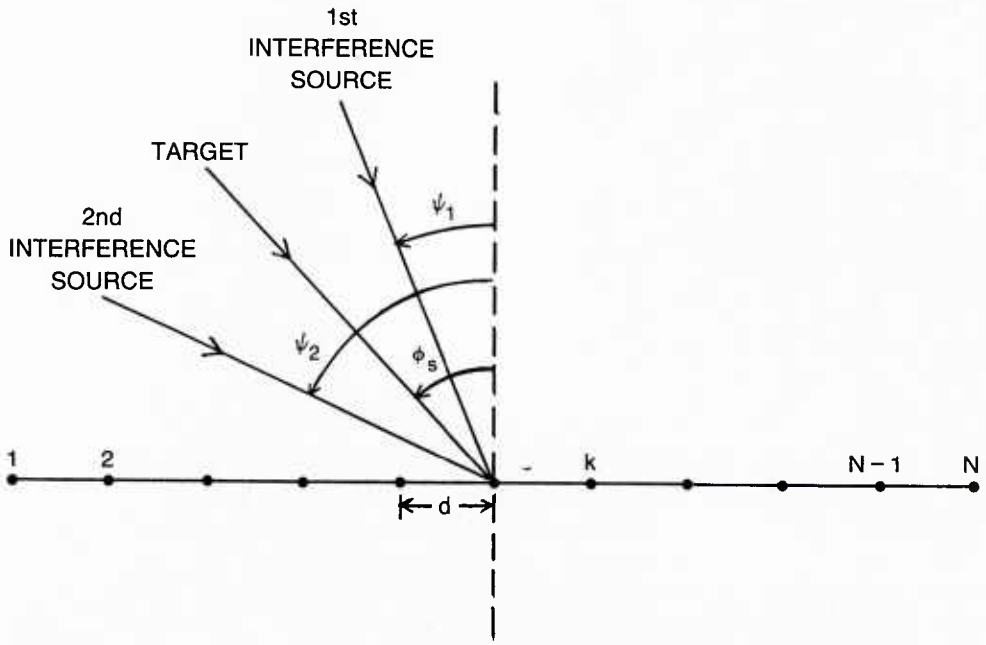

Fig. 1 — Array geometry

d is the element spacing,
λ is the wavelength, and
$j = \sqrt{-1}$.

The signal is assumed to be processed in time-sampled, digitized inphase I and quadrature Q channels. Each complex time sample across the array comprises a snapshot. Throughout this study the antenna element spacing is $\lambda/2$. The objective is to estimate ϕ_s, the angle of arrival of the desired signal measured from the beam pointing direction, in the presence of internal noise and high-power, high-duty-cycle external interference sources. We assume that the target signal occurs in a single range cell whereas the interference signals appear in many range cells.

In general the angle estimation technique consists of two measurements. The first one is used to determine the monopulse error calibration curve. It uses the total interference signal appearing at each antenna array element from which the covariance matrix can be computed. The second measurement, which is used to determine the target angle, is described later. It uses the total signal received in the presence of both target and interference sources.

In the first measurement, the covariance matrix R is estimated from many range cells of data in the absence of a target signal. Here we first assume that R is known exactly, which is equivalent to averaging over an infinite number of snapshots. In Section V we discuss the effect of using an R estimated from a finite number of snapshots on the angle estimation accuracy. Based on the known interference scenario, the total interference appearing at the kth array element is given by

$$Q_k = \sum_{i=1}^{N_J} r_i \, e^{j(2\pi/\lambda)(k-1)d \sin \psi_i} + n_k. \tag{2}$$

The pq-element of the covariance matrix is obtained by applying the expected value operator $\mathscr{E}$:

$$R_{pq} = \mathscr{E}[Q_p \, \overline{Q}_q^T] \tag{3}$$

where $\overline{(\cdot)}$ denotes the complex conjugate and T is the transpose operation. The covariance matrix can be explicitly expressed in the form,

$$R = \sum_{i=1}^{N_J} \sigma_i^2 \begin{bmatrix} 1 & e^{-j(2\pi/\lambda)d \sin \psi_i} & e^{-2j(2\pi/\lambda)d \sin \psi_i} & \cdots \\ e^{j(2\pi/\lambda)d \sin \psi_i} & 1 & e^{-j(2\pi/\lambda)d \sin \psi_i} & \cdots \\ \cdot & \cdot & 1 & \cdots \\ \cdot & \cdot & \cdot & \cdots \\ \cdot & \cdot & \cdot & \cdots 1 \end{bmatrix}$$

$$+ \sigma_n^2 \begin{bmatrix} 1 & 0 & \cdot & 0 \\ 0 & 1 & 0 & \cdot \\ \cdot & \cdot & \cdot & \cdot \\ 0 & \cdot & \cdot & 1 \end{bmatrix}. \tag{4}$$

where σ_i^2 is the noise power of the ith interference source, and σ_n^2 is the thermal noise power, which is assumed to be the same for each element.

The tracking beams are based on selecting an adjacent pair of orthogonal, uniform illumination beams that are generated by a Butler matrix beamformer transformation [2]. The resultant sum beam weight vector S_0 and the difference beam weight vector D_0 at the output of the Butler beamformer are equivalent to cosine illuminations.

For a vector E of the received echoes on the N-element array, the adapted sum and difference beam outputs obtained by applying conventional beam weighting S_0 and D_0 to the spatial filtered output residue signal vector, E_f ($E_f = R^{-1}E$), are given by

$$\Sigma = S_o^T \cdot R^{-1} \, E \tag{5}$$

and

$$\Delta = D_o^T \, R^{-1} \, E. \tag{6}$$

As a result of the Butler matrix transformation, Δ is 90° out of phase with Σ and the desired monopulse ratio is the imaginary part of (Δ/Σ), denoted by $\mathrm{Im}(\Delta/\Sigma)$. For calibration, $\mathrm{Im}(\Delta/\Sigma)$ is calculated by letting the vector E be a steering vector steered across the beam to give the distorted monopulse curve in the tracking angle region. If there is no external interference source, there is no distortion. The difference pattern has a null at the beam center where the sum pattern peaks (Figs. 2(a) and 2(b)). The monopulse error curve is ideally linear over the tracking region within the 3 dB beamwidth (θ_{BW}), as shown in Fig. 2(c) for an 8-element array.

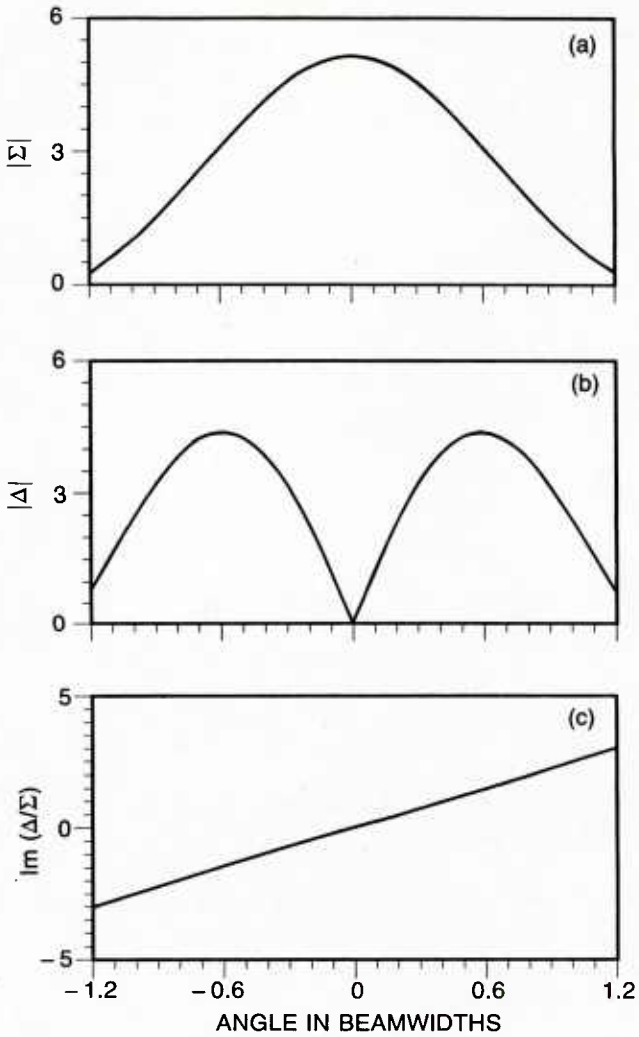

Fig. 2 — No interference: (a) sum pattern; (b) difference pattern; (c) monopulse error curve

The calibration curves for estimating the angle of arrival in the presence of external interference are obtained as follows. Assume that E is the desired steering vector,

$$E = \begin{bmatrix} 1 \\ e^{j(2\pi/\lambda)\, d\, \sin\phi_s} \\ \cdot \\ \cdot \\ e^{j(2\pi/\lambda)\,(N-1)d\, \sin\phi_s} \end{bmatrix}. \tag{7}$$

which is a function of angle of arrival only. Substituting Eq. (7) into Eqs. (5) and (6), one obtains the ratio $\mathrm{Im}(\Delta/\Sigma)$ as a function of direction of arrival ϕ_s. For example, consider a covariance matrix

being constructed based on an interference source located at 0.5 θ_{BW} (θ_{BW} = 16.8815° for an 8-element array). The adapted Σ and Δ patterns are obtained by using Eqs. (5) and (6) and are shown in Figs. 3(a) and 3(b). Note that a notch is placed at the corresponding interference source location in both patterns that are distorted from the interference-free cases (Figs. 2(a) and 2(b)). Figure 3(c) shows the ratio Im(Δ/Σ) as a function of ϕ_s. The slope of the monopulse error curve is significantly different from that shown in Fig. 2(c). It has a singular point at the interference source location. In the two-source case where an additional interference source is placed at $-0.5\ \theta_{BW}$, the adapted Σ and Δ patterns are depicted in Figs. 4(a) and 4(b), respectively. Note that both patterns have nulls at these two source locations. The monopulse error curve shown in Fig. 4(c), also different from Fig. 2(c), has two singular points where the interference sources are located. The distorted monopulse error curves computed as described above are used as the calibration curve in estimating the angle of arrival when the received signal is contaminated by the interference sources.

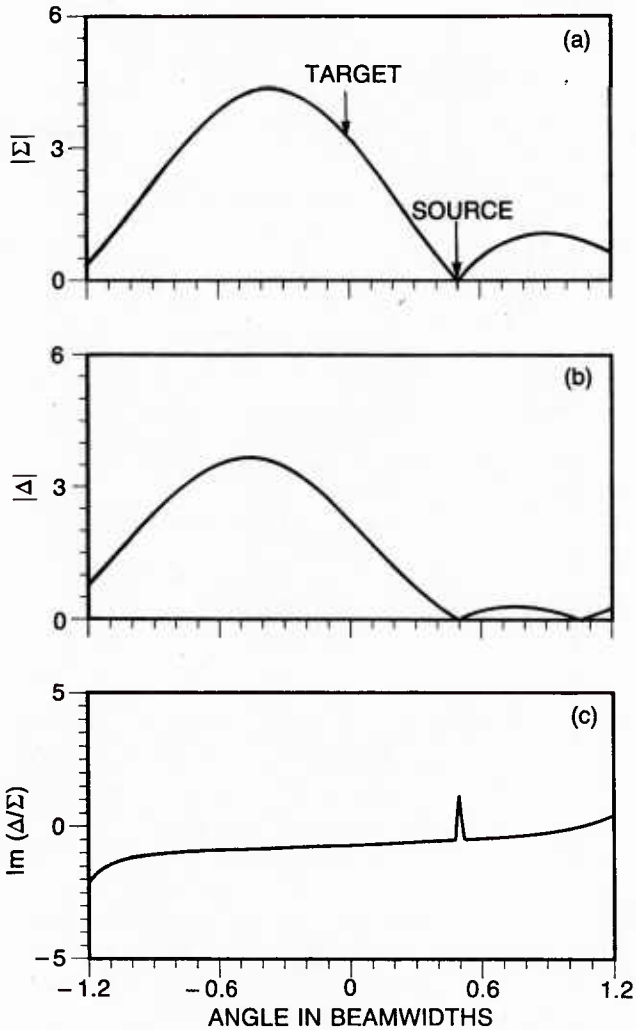

Fig. 3 — One interference source at 0.5 beamwidth: (a) sum pattern; (b) difference pattern; (c) monopulse error curve

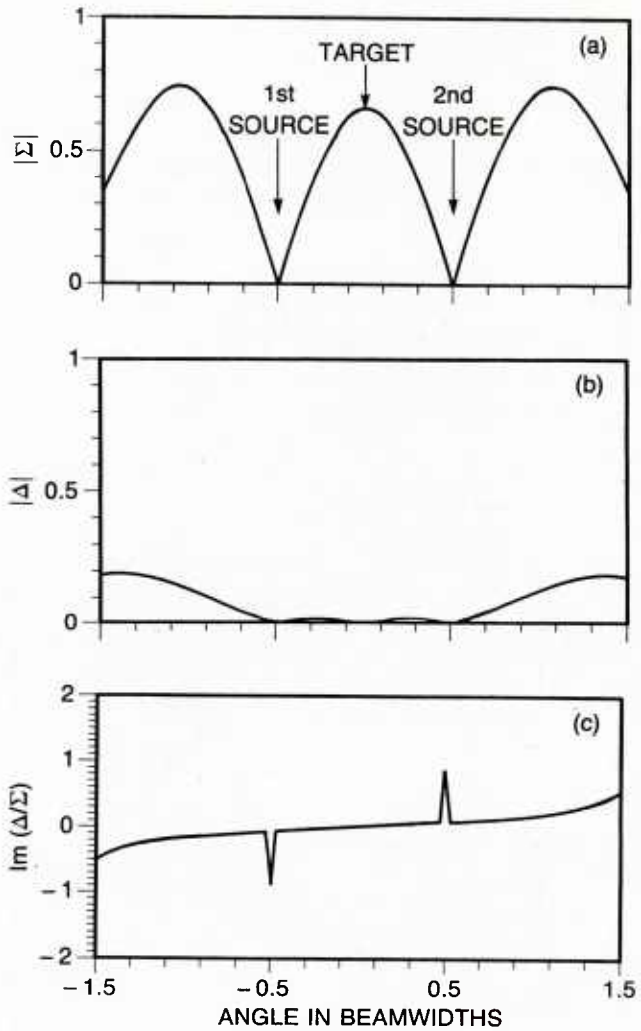

Fig. 4 — Two interference sources at 0.5 and −0.5 beamwidth, respectively: (a) sum pattern; (b) difference pattern; (c) monopulse error curve

The second measurement involves the received signals consisting of the returns from the interference sources and the desired signal. Substituting the vector E, as given by

$$E = [X_1\ X_2\ \ldots X_N]^T.$$

where X_k is defined in Eq. (1), into Eqs. (5) and (6), one can calculate the distorted ratio $\mathrm{Im}(\Delta/\Sigma)$. The corresponding angle of arrival ϕ_s in the interference environment can be estimated from the ratio $\mathrm{Im}(\Delta/\Sigma)$ based on the calibration curve obtained in the first measurement described above.

III. THE CRAMER-RAO BOUND ON ANGLE ESTIMATION ERROR

The Cramer-Rao (C-R) bound is the lower bound on the variance of any unbiased estimator. It is useful to compare the performance of an estimation procedure with this bound. Brennan [3], using

the C-R bound on angle estimation error, has determined the limit on angle estimation accuracy for a target in the presence of internal noise with known signal amplitude but unknown phase. For a target with an unknown amplitude that is Rayleigh distributed, and an unknown phase that is uniformly distributed between 0 and 2π, McGarty [4] has derived the C-R bound in the presence of more than one interference source based on the specific interference model that was considered in obtaining the covariance matrix.

A general case consisting of unknown signal amplitude, phase, and angles of arrival is considered here. The problem of angle estimation is similar to that described in Ref. 5 in terms of a Doppler velocity estimation process. In the Appendix we show that for K independent samples of $\mathrm{Im}(\Delta/\Sigma)$ the C-R bound for the estimation error of $\sin \phi_s$ is given by (Eq. (A10))

$$(\sigma_{\mu'})^2 \geq \frac{1}{SK} \left[\frac{C\bar{C}}{C\bar{C}(D + \bar{D}) - A\bar{A}(C + \bar{C})} \right], \tag{8}$$

where

$$\mu' = \sin \phi_s,$$

$$W^T = [1 \; e^{j(2\pi/\lambda)d} \; e^{j(2\pi/\lambda)2d} \ldots e^{j(2\pi/\lambda)(N-1)d}],$$

$$C = W^T R^{-1} \bar{W},$$

$$A = W^T B R^{-1} \bar{W},$$

$$D = W^T B R^{-1} \bar{B} \bar{W},$$

$$B = \begin{bmatrix} 0 & 0 & \cdot & \cdot & \cdot & \cdot \\ \cdot & j(2\pi/\lambda)d & 0 & \cdot & \cdot & \cdot \\ \cdot & \cdot & j(2\pi/\lambda)2d & 0 & & \\ 0 & 0 & \cdot & \cdot & \cdot & 0 \\ 0 & 0 & \cdot & \cdot & \cdot & j(2\pi/\lambda)(N-1)d \end{bmatrix},$$

S is the input signal power in each antenna element, and

K is the number of independent samples of Im (Δ/Σ) processed.

This expression is for an array of N identical antenna elements with equal spacing d.

A. Single Interference Source:

The C-R bound on rms $\sin \phi_s$ estimate error normalized to $\sin \theta_{BW}$, or $\sigma_{\mu'}/\sin \theta_{BW}$, which is denoted by σ_μ, is calculated as a function of angular separation between the target and the interference

source normalized to θ_{BW}. The scenario consists of a target with 10 dB signal-to-noise ratio (S/N_0) and an interference source with 30 dB interference-to-noise ratio (I/N_0). Figure 5(a) shows the C-R bound for an 8-element array when four different values of K (K = 1, 8, 16, and 32) are processed. It demonstrates that higher precision in angle estimation accuracy is achieved as more samples are averaged before estimating the angle of arrival. The angle estimation error varies very little when the angular separation between the interference source and the target becomes slightly greater than one beamwidth. Generally this error increases as the interference source approaches the target direction. The C-R bound on σ_{ϕ_s}, which is defined as the angle estimation error in beamwidths, is shown in Fig. 5(b) to be in excellent agreement with Fig. 5(a) for the same scenario. The vertical axis in all the plots that appear later in terms of σ_μ can be viewed approximately as the angle estimation error in beamwidths.

Figure 6 shows the results for three different array sizes when 32 independent samples are processed. The variation in angle estimation error with the angular separation is similar for different array sizes. Also, the error incurred in the angle estimation is less for larger array size. Figure 7 shows the C-R bound on σ_μ of a 10 dB S/N_0 target using an 8-element array as a function of angular separation from an interference source with I/N_0 of 10, 20, 30, 40, and 50 dB based on 32 independent samples. It shows that the angle estimation error becomes more severe as the power of the interference source increases. For an angular separation of more than approximately one beamwidth, the rms error levels off and the power of the interference source does not significantly affect the estimation error.

The scenario in Fig. 8 is identical to that in Fig. 7 except the target has a S/N_0 of 0 dB and the interference source has four different values of I/N_0 (I/N_0 = 0, 10, 20, and 30 dB). Again with an angular separation of slightly greater than one beamwidth, the estimation error is the same for all I/N_0 power levels. A comparison of Fig. 8 with Fig. 7 shows that better angle estimation is achieved for higher S/N_0 with the same I/S ratio in both cases. Figure 9 is the same as Fig. 8 except N = 16. It is demonstrated by comparing these two figures that a smaller error is obtained for a larger array size with the identical target and interference source scenarios.

B. Two Interference Sources:

In these calculations, it is assumed that the target is at the center of the antenna mainbeam. The scenario considered here is that the two interference sources of equal power are located symmetrically with respect to the target. Figure 10 shows the C-R bound of σ_μ plotted as a function of angular separation between the target and one of the two symmetrically located interference sources, normalized to θ_{BW}, for four different values of K (K = 1, 8, 16, and 32). The parameters used in Fig. 10 are: N = 8, S/N_0 = 10 dB, and I/N_0 = 30 dB for both interference sources. The error is reduced as the interference sources simultaneously move away from the target (from 0.1 to 1.0 θ_{BW}). The error approaches a constant value as the interference sources are more than one beamwidth from the target.

IV. ANGLE ESTIMATION ERROR BASED ON SIMULATION RESULTS

The method described in Section II is used to estimate the angle of arrival in the presence of mainbeam interference. The normalized angular error is then compared with the bound. The received signal X_k as given in Eq. (1) is simulated for each sample of a run. Random complex Gaussian variables are generated to represent interference sources and receiver noise. The Σ and Δ beam

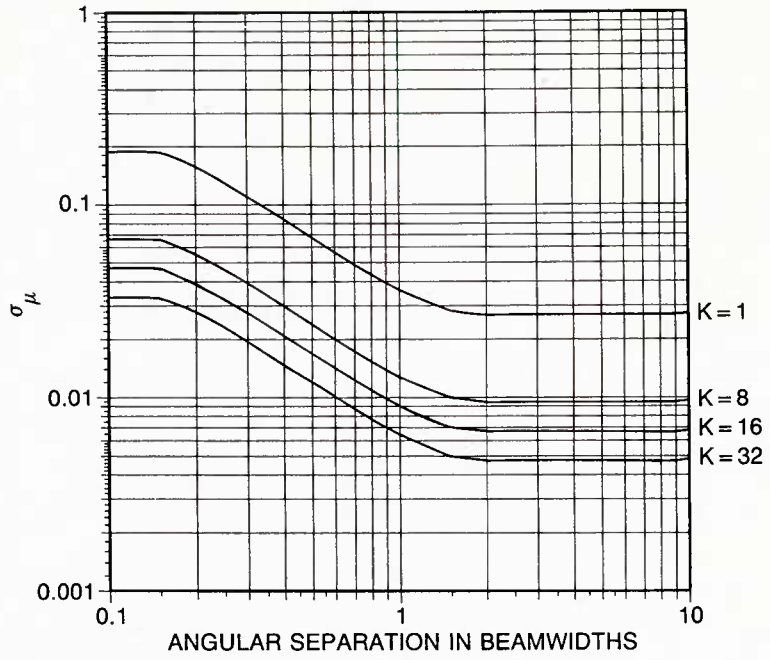

(a)

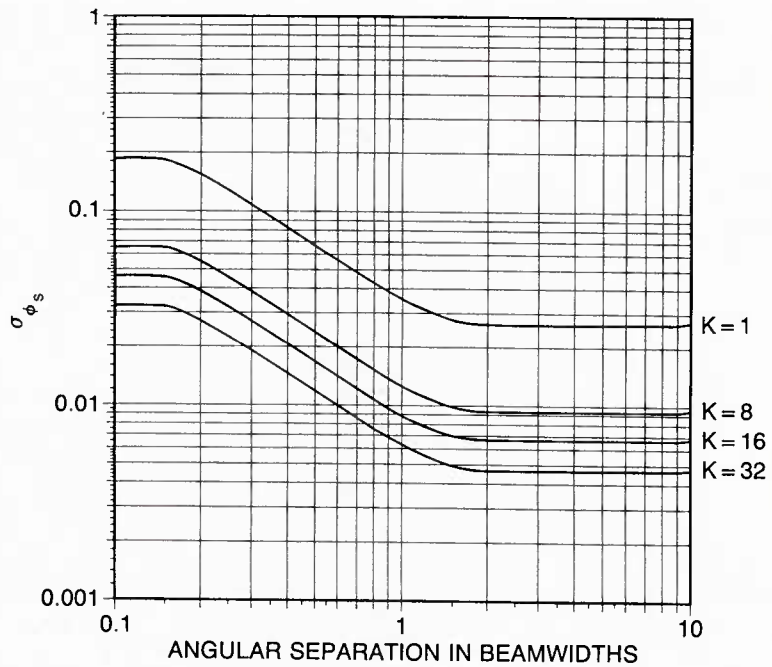

(b)

Fig. 5 — (a) The Cramer-Rao bound of σ_μ, (b) The Cramer-Rao bound of σ_{ϕ_s}, as a function of angular separation for different values of K: $N = 8$; $S/N_0 = 10$ dB; $I/N_0 = 30$ dB.

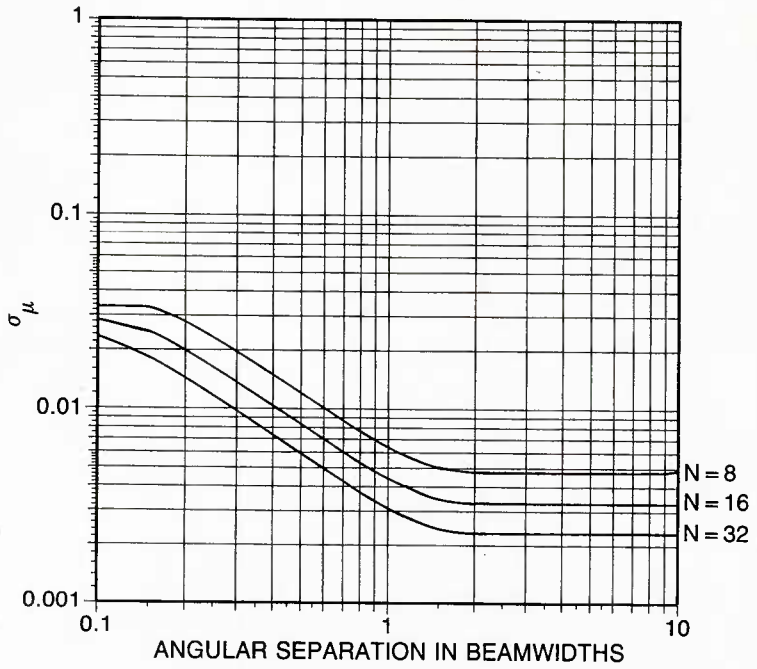

Fig. 6 — The Cramer-Rao bound of σ_μ as a function of angular separation for different values of N: $K = 32$; $S/N_0 = 10$ dB; $I/N_0 = 30$ dB.

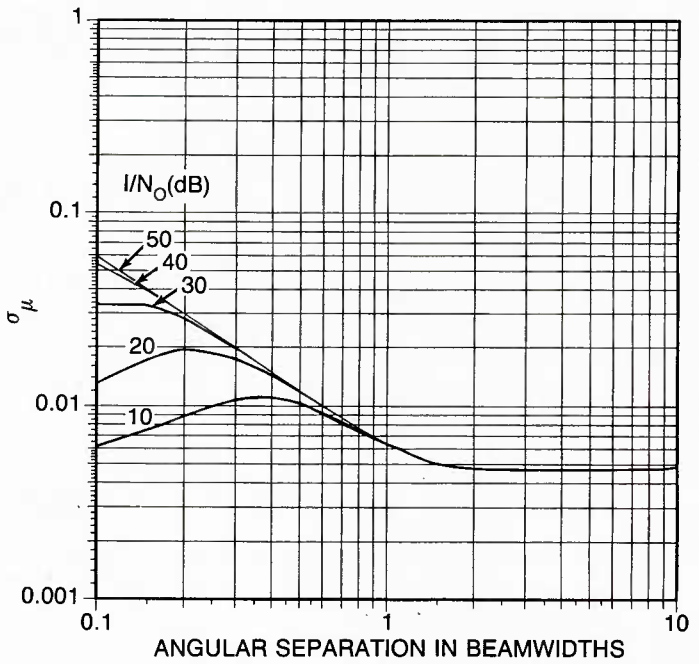

Fig. 7 — The Cramer-Rao bound of σ_μ as a function of angular separation for different values of I/N_0: $N = 8$; $K = 32$; $S/N_0 = 10$ dB.

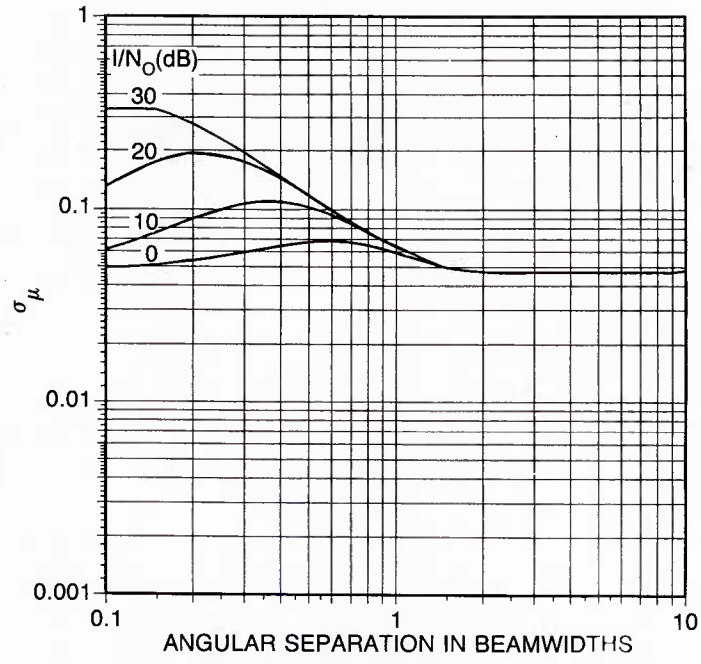

Fig. 8 — The Cramer-Rao bound of σ_μ as a function of angular separation for different values of I/N_0: $N = 8$; $K = 32$; $S/N_0 = 0$ dB.

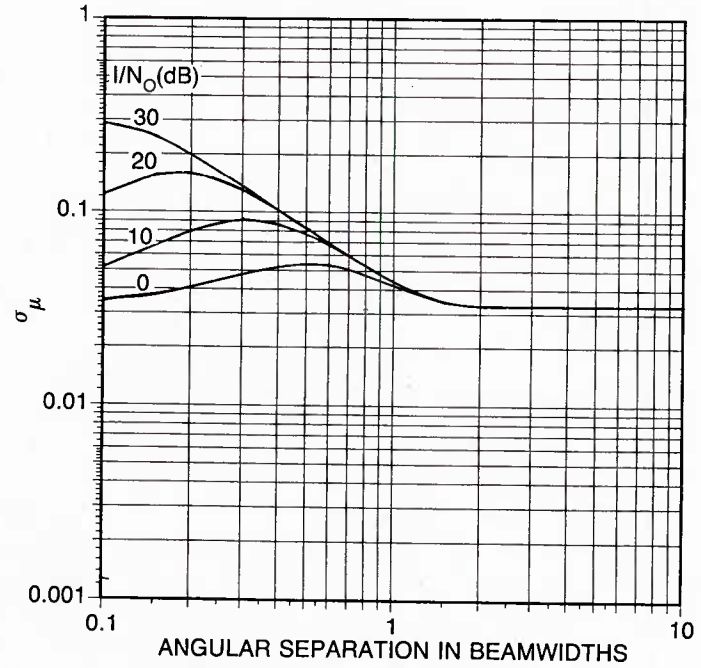

Fig. 9 — The Cramer-Rao bound of σ_μ as a function of angular separation for different values of I/N_0: $N = 16$; $K = 32$; $S/N_0 = 0$ dB.

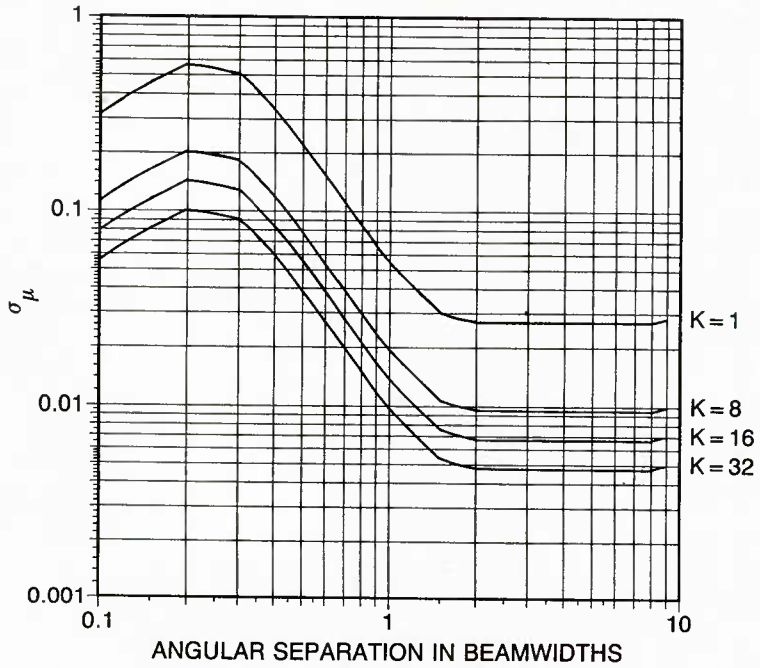

Fig. 10 — The Cramer-Rao bound of σ_μ as a function of angular separation for different values of K in the presence of two interference sources with target at the beam center: $N = 8$; $S/N_0 = 10$ dB; $I_1/N_0 = 30$ dB; $I_2/N_0 = 30$ dB.

returns are obtained by using Eqs. (5) and (6) for each run, and the ratio $\mathrm{Im}(\Delta/\Sigma)$ is calculated. Finally, K-independent samples of the ratio are averaged before the target angle is estimated by using the calibration curves obtained from the first procedure of the estimation technique described in Section II. The results presented here are based on repeating the above process of angle estimation 100 times.

In the single-source case the following scenario is assumed. An antenna array with 8 elements is used to receive the signal consisting of the returned echo from a target with $S/N_0 = 10$ dB and an interference source with $I/N_0 = 30$ dB. The interference source location is chosen first and the target direction is varied within the mainbeam. Figures 11(a), 11(b), 11(c), and 11(d), respectively, show the results for the selected interference source locations (0.2, 0.5, 0.7, and 0.9 θ_{BW}, for example) as the target direction is varied from the interference source, first toward the beam center and then away from it. The solid lines are the theoretical C-R bounds on σ_μ, and the individual data points are from the simulation. Four different values of K ($K = 1$, 8, 16, and 32) are used to demonstrate the effects on the angle estimation accuracy. All the simulated points are near the C-R bounds for all values of K tested. Figures 12(a), 12(b), 12(c), and 12(d), for the four different values of K, respectively, show the combined results with the interference source locations varying from 0.1 to 0.9 θ_{BW} with a step of 0.1 θ_{BW}. The simulated points of the same symbol correspond to the scenario with a fixed interference source location and various target locations. Here the target is located in the mainbeam but not necessarily at the mainbeam center. Figure 13 shows the results for the case when the target is assumed at the mainbeam center and the interference source location is varied from 0.2 to 0.9 θ_{BW} with an increment of 0.1 θ_{BW} for four different values of K ($K = 1$, 8,

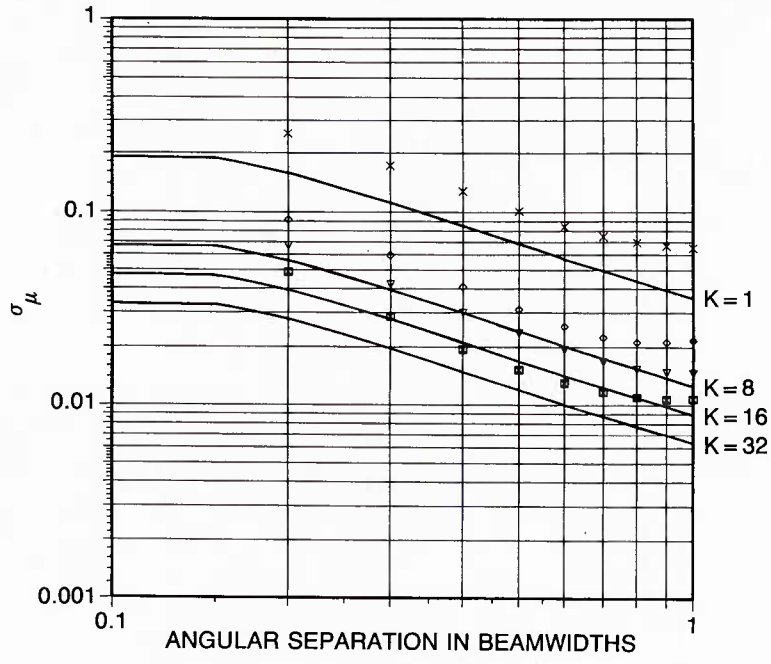

(a)

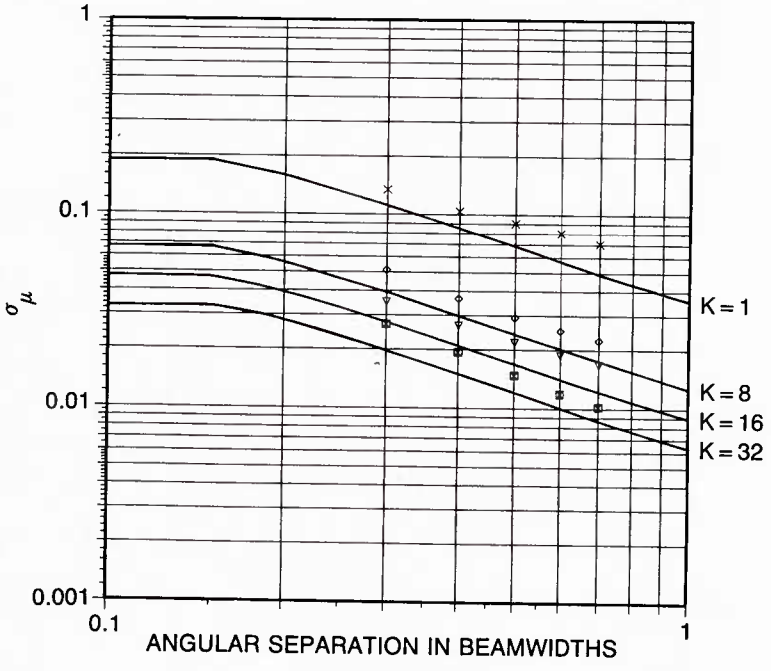

(b)

Fig. 11 — The Cramer-Rao bound (——) and the simulated data points: K = 1 (xxx), K = 8 (◇ ◇ ◇), K = 16 (▽ ▽ ▽), and K = 32 (⊠⊠⊠), of σ_μ as a function of angular separation: N = 8; S/N_0 = 10 dB; I/N_0 = 30 dB. Interference source is at: (a) 0.2, (b) 0.5, (c) 0.7, and (d) 0.9 beamwidth.

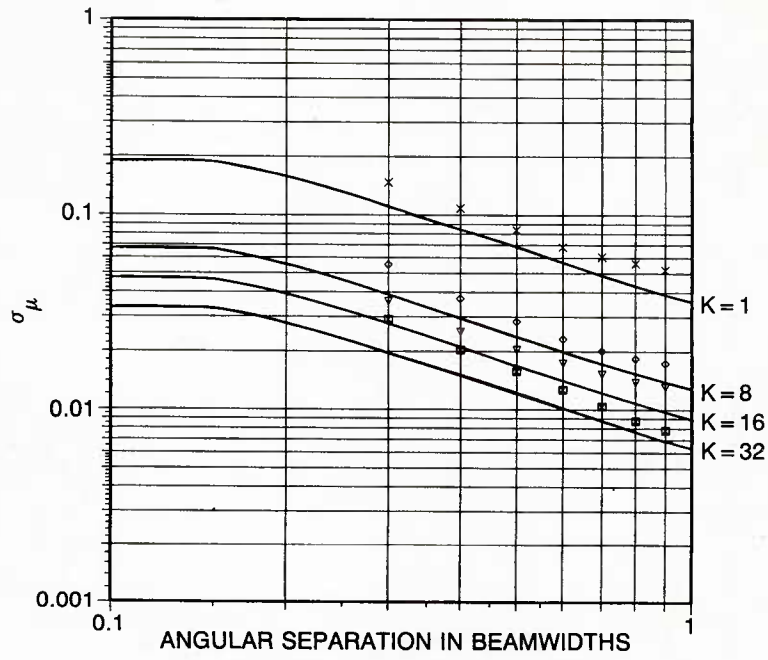

(c)

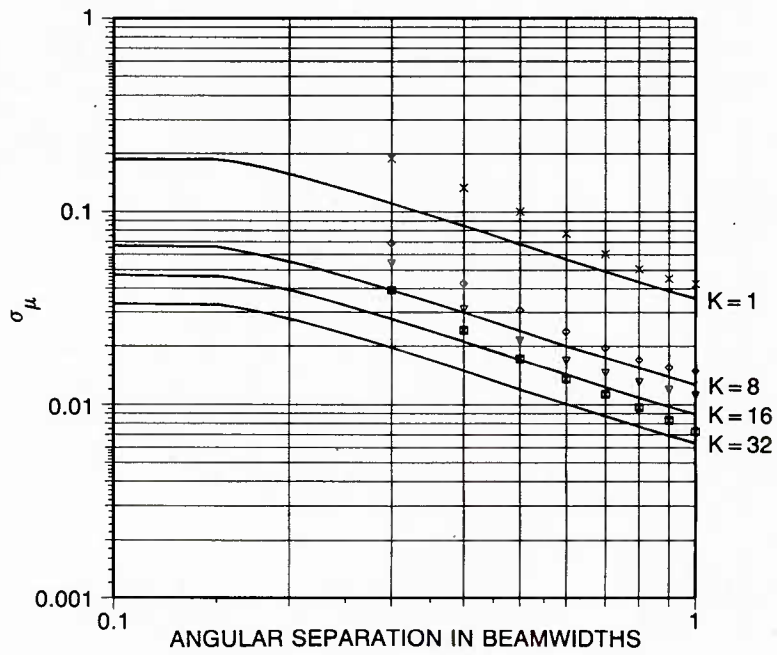

(d)

Fig. 11 (Continued) — The Cramer-Rao bound (——) and the simulated data points: $K = 1$ (xxx), $K = 8$ ($\diamond\ \diamond\ \diamond$), $K = 16$ ($\nabla\ \nabla\ \nabla$), and $K = 32$ ($\boxtimes\ \boxtimes\ \boxtimes$), of σ_μ as a function of angular separation: $N = 8$; $S/N_0 = 10$ dB; $I/N_0 = 30$ dB. Interference source is at: (a) 0.2, (b) 0.5, (c) 0.7, and (d) 0.9 beamwidth.

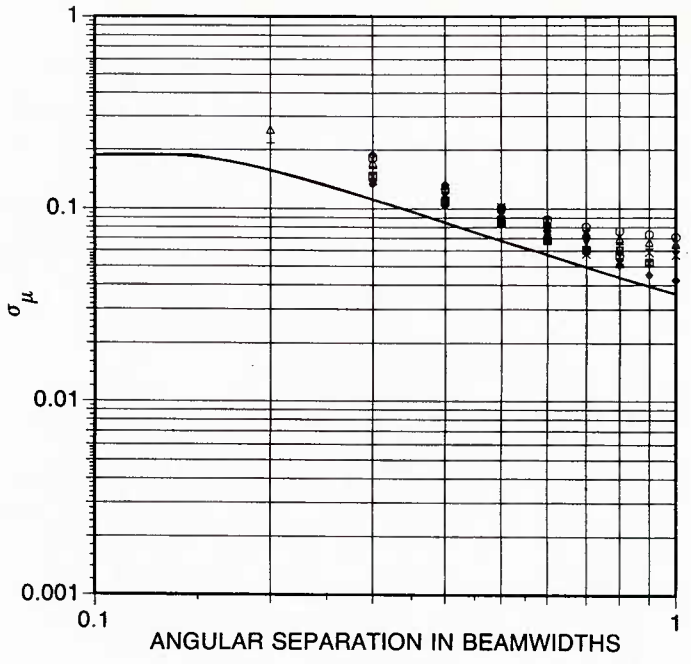

(a)

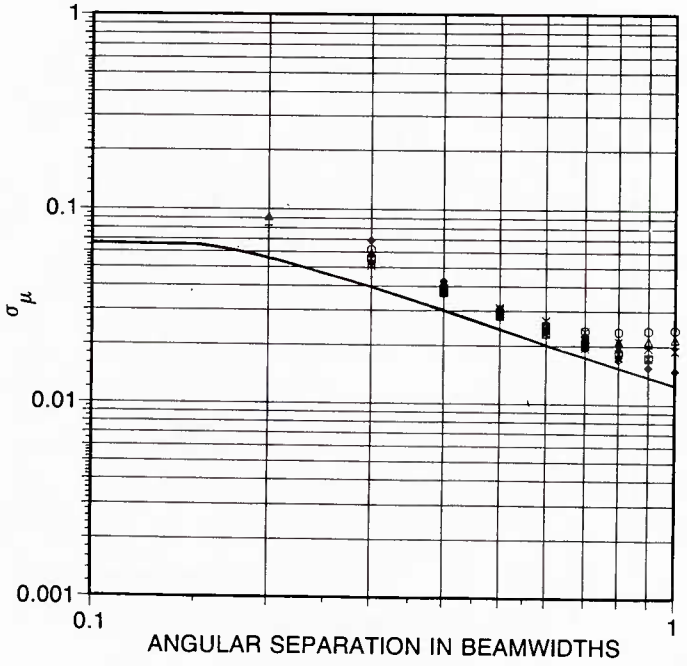

(b)

Fig. 12 — The Cramer-Rao bound (——) and the simulated data points for: (a) $K = 1$, (b) $K = 8$, (c) $K = 16$, and (d) $K = 32$, of σ_μ as a function of angular separation: $N = 8$; $S/N_0 = 10$ dB; $I/N_0 = 30$ dB. Interference source location is varied from 0.1 to 0.9 beamwidth.

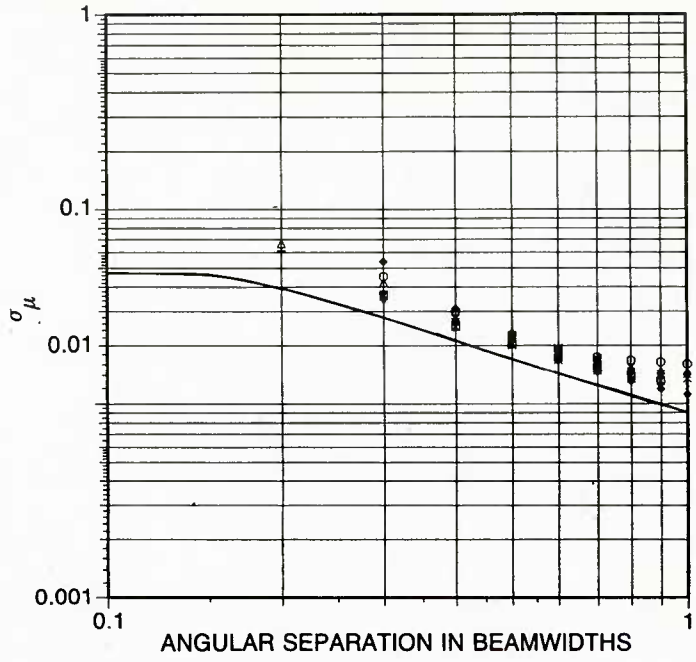

(c)

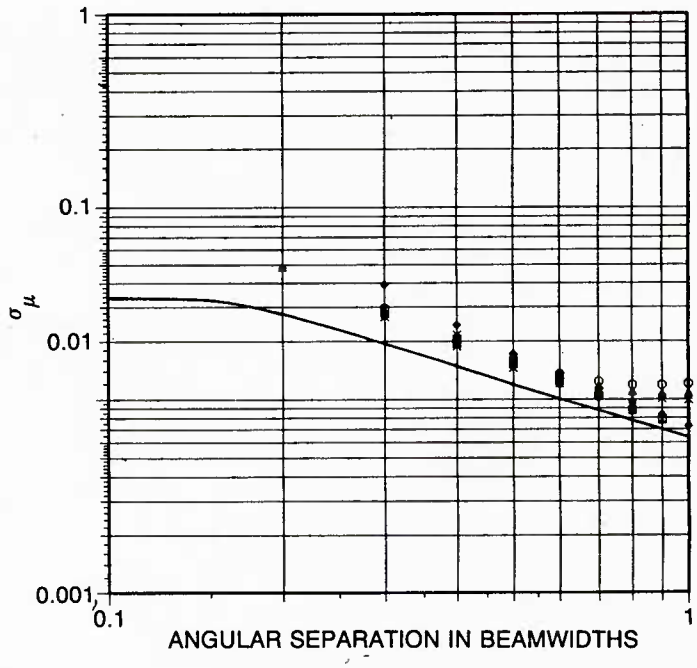

(d)

Fig. 12 (Continued) — The Cramer-Rao bound (——) and the simulated data points for: (a) $K = 1$, (b) $K = 8$, (c) $K = 16$, and (d) $K = 32$, of σ_μ as a function of angular separation: $N = 8$; $S/N_0 = 10$ dB; $I/N_0 = 30$ dB. Interference source location is varied from 0.1 to 0.9 beamwidth.

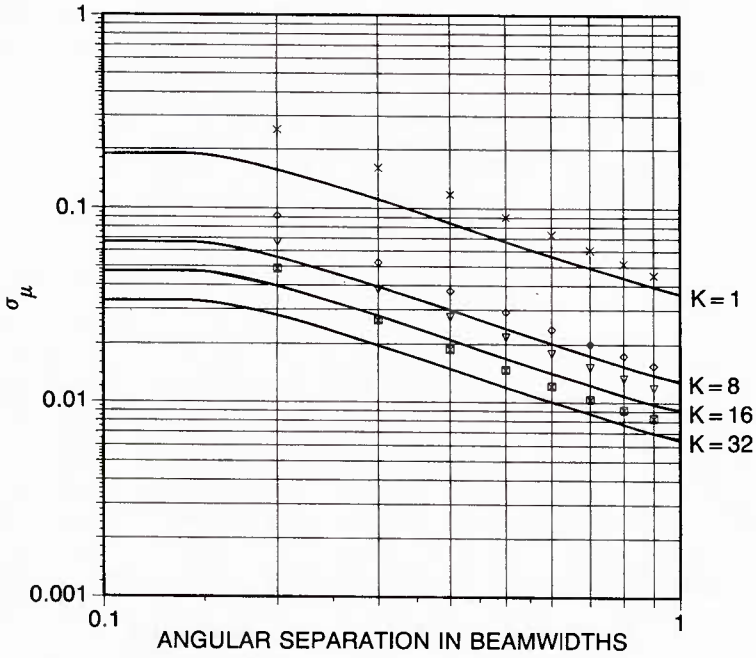

Fig. 13 — The Cramer-Rao bound (——) and the simulated data points: $K = 1$ (xxx), $K = 8$ ($\diamond\diamond\diamond$), $K = 16$ ($\nabla\nabla\nabla$), and $K = 32$ ($\boxtimes\boxtimes\boxtimes$), of σ_μ as a function of angular separation with target at the beam center: $N = 8$; $S/N_0 = 10$ dB; $I/N_0 = 30$ dB.

16, and 32). The C-R bound of the angle estimation error is also plotted in Fig. 13. The angular error obtained from the estimation procedure described here for the single-source case is shown to be quite close to the C-R bound derived here. The error is less than 0.1 θ_{BW} for $K \geq 8$.

Simulation is also performed for the two-source case. The scenario considered here includes a target at the mainbeam center and two interference sources symmetrically located on both sides of the target direction within the mainbeam. The parameters used here are the same as in the single-source case, except there are two interference sources with equal I/N_0 of 30 dB. Figure 14 shows the simulation results and the C-R bounds. For an angular separation between the target and one of the symmetrically located interference sources greater than 0.5 θ_{BW}, the simulated points obtained by the estimation method described here are within 0.1 θ_{BW} for $K \geq 8$ and are close to the C-R bound. As the separation between the target and the interference sources becomes equal to or less than 0.5 θ_{BW}, the accuracy of angle estimation starts to degrade.

V. EFFECTS OF ESTIMATING THE COVARIANCE MATRIX

So far we have assumed that the covariance matrix is obtained by averaging over an infinite number of range cells. In practice, the covariance matrix must be estimated from a finite number of snapshots. The effect of the accuracy of the estimated covariance matrix on the accuracy of the angle estimation is briefly examined here.

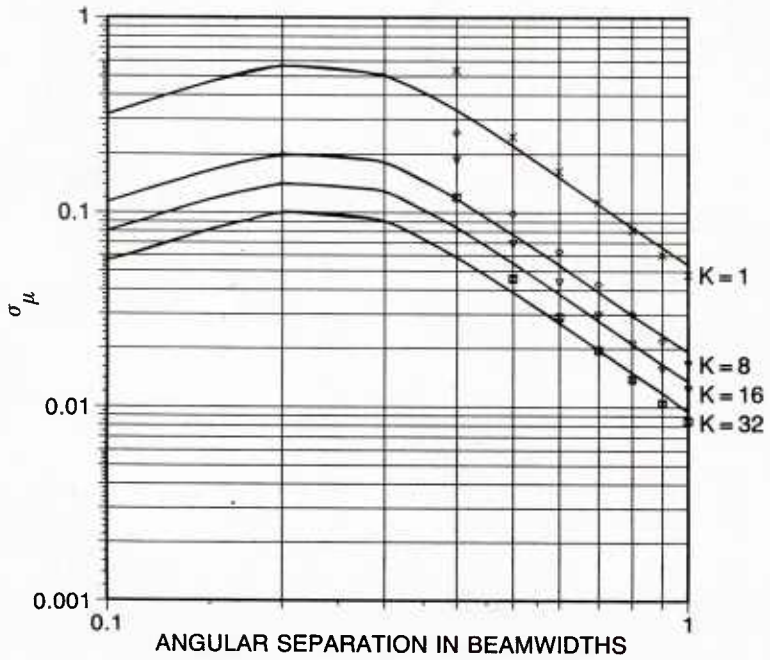

Fig. 14 — The Cramer-Rao bound (——) and the simulated data points: $K = 1$ (xxx), $K = 8$ ($\diamond\,\diamond\,\diamond$), $K = 16$ ($\nabla\,\nabla\,\nabla$), and K = 32 ($\boxtimes\,\boxtimes\,\boxtimes$), of σ_μ as a function of angular separation in the presence of two interference sources with target at the beam center: $N = 8$; $S/N_0 = 10$ dB; $I_1/N_0 = 30$ dB; $I_2/N_0 = 30$ dB.

First, the covariance matrix R is estimated by using 32 snapshots. Procedures for estimating the angle of arrival of the desired signal previously described are repeated by using the estimated rather than the ideal value of R. Figure 15(a) shows the results obtained for an interference source located at 0.5 θ_{BW} with the same scenario as that used in Fig. 11(b). Solid lines are the C-R bounds, and the individual data points are from the simulation. The simulated angle errors are far above the C-R bounds.

Next, 256 snapshots are used for estimating R. Figure 15(b) shows the results. Note that the errors in angle estimation are much lower than those shown in Fig. 15(a). As the number of snapshots increase, the angle estimation accuracy improves and approaches what is shown in Fig. 11(b) for an idealized covariance matrix. Also, more snapshots are required to approach the bound as the angular separation decreases.

VI. SUMMARY

An investigation has been performed on estimating the angle of arrival of a desired signal in the presence of mainbeam interference. Adaptive antenna arrays are incorporated to form adapted sum and difference beams in which the interference signals are suppressed. Monopulse error curves are then obtained, providing the necessary distortion correction curves across the entire mainbeam tracking angle region. New C-R bounds on the angle estimation error are derived with generalized assumptions on the signal amplitude and phase. The bounds previously derived by others are valid

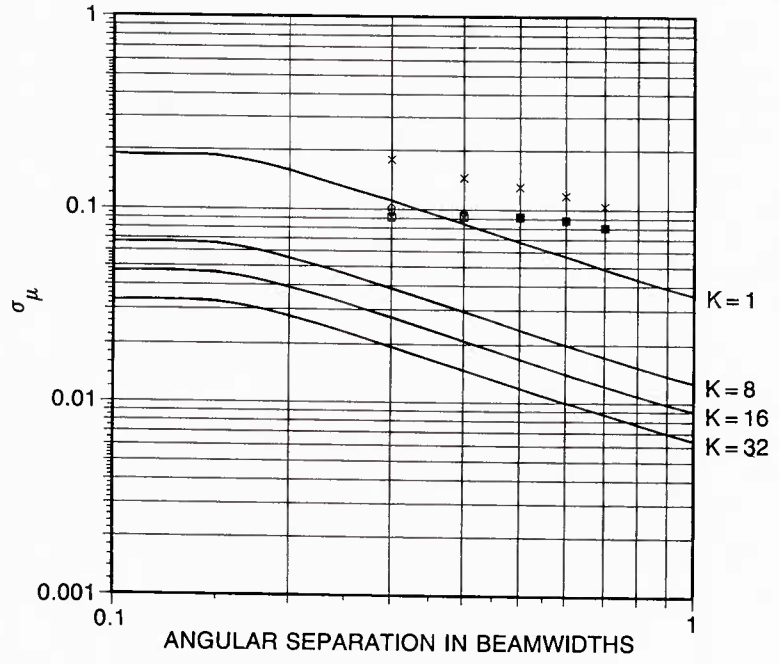

(a)

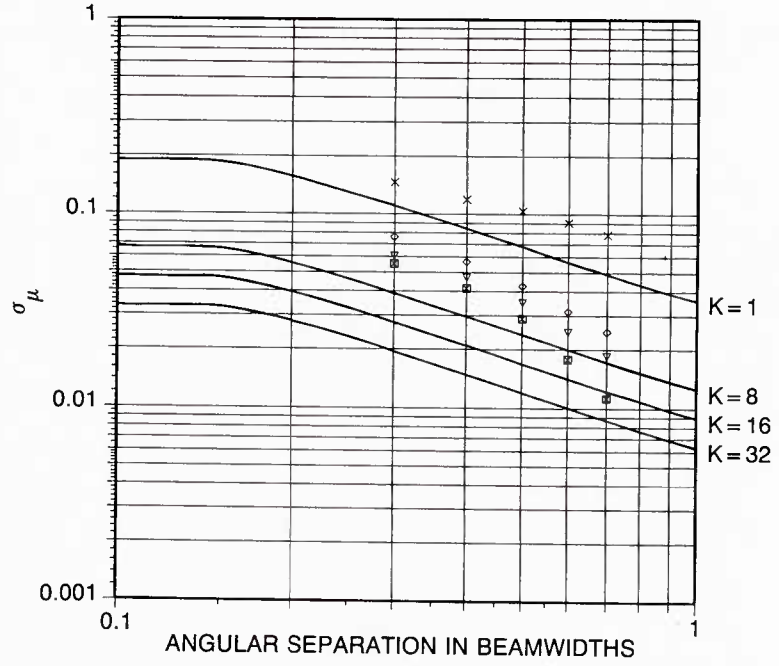

(b)

Fig. 15 — The Cramer-Rao bound (——) and the simulated data points: $K = 1$ (xxx), $K = 8$ (◇◇◇), $K = 16$ (▽▽▽) and $K = 32$ (⊠⊠⊠), of σ_μ as a function of angular separation for an interference source located at 0.5 beamwidth: $N = 8$; $S/N_0 = 10$ dB; $I/N_0 = 30$ dB. R is estimated from (a) 32; (b) 256 samples.

under different conditions. With these generalized assumptions on the signal characteristics, a Monte Carlo simulation is performed based on the estimation procedure described herein to determine the angle estimation error. These errors are compared with the C-R bounds. Good performance is shown for sufficient S/N_0 and angular separation between the target and the interference sources.

For the case of an 8-element array with a single interference source, the angle estimation error is within 0.1 θ_{BW} when the angular separation is equal or greater than 0.2 θ_{BW} and at least eight independent samples of the monopulse measurement $\mathrm{Im}(\Delta/\Sigma)$ are processed. To achieve the same accuracy in angle estimation for the two-source case, the angular separation must be greater than 0.5 θ_{BW}.

The issue of the effect of estimating the covariance matrix from a finite number of snapshots on the angle estimation accuracy is also briefly addressed. It is shown that the accuracy in angle estimation is greatly affected by the estimated covariance matrix. In general, more snapshots are needed to approach the bounds as the angular separation between the target and the interference source decreases.

VII. REFERENCES

1. R. C. Davis, L. E. Brennan, and L. S. Reed, "Angle Estimation with Adaptive Arrays in External Noise Fields," *IEEE Trans. Aerosp. Electron. Syst.* **AES-12**, 179-186 (1976).

2. W. F. Gabriel, "A High-Resolution Target-Tracking Concept Using Spectral Estimation Techniques," NRL Report 8797, May 1984.

3. L. E. Brennan, "Angular Accuracy of a Phased Array Radar," *IRE Trans. Ant. Propag.* **AP-9**, 268-275 (1961).

4. T. P. McGarty, "The Effects of Interference Signals on the Performance of Angle of Arrival Estimates," *IEEE Trans. Aerosp. Electron. Syst.* **AES-10**, 70-77 (1974).

5. F. C. Lin and B. H. Cantrell, "Bounds on Doppler Frequency Estimation in Correlated Nonstationary Gaussian Noise," NRL Report 9140, Aug. 1988.

Appendix

Let X_i be an N-dimensional complex signal vector representing the ith sample of the signal received by the N-element linear antenna array. The received signal vector X_i, composed of a signal component s_i and a noise component n_i, is given by

$$X_i = s_i + n_i = b\ W + n_i, \tag{A1}$$

where n_i is a complex zero-mean Gaussian process with covariance matrix R, b is the unknown complex signal strength, and W is the steering vector. For an N-element linear antenna array of identical elements and uniform spacing d, the steering vector is written in terms of Δ, the phase shift from element to element, owing to the angle of arrival ϕ_s:

$$W^T = [1\ e^{j\Delta}\ e^{2j\Delta} \ldots e^{(N-1)j\Delta}], \tag{A2}$$

where T denotes the transpose, j is the square root of -1, $\Delta = (2\pi/\lambda)d \sin \phi_s$, and λ is the wavelength. The vector X_i has a conditional probability density

$$p\ (X_i \mid \Theta) = \frac{1}{\pi^N \mid R \mid} \exp \{- \overline{(X_i - bW)}^T\ R^{-1}\ (X_i - bW)\}, \tag{A3}$$

where Θ represents the unknown parameters $\mu'(\mu' = \sin \phi_s)$, b, and $\bar{b}$; $\overline{(\cdot)}$ denotes the complex conjugate; and $\mid R \mid$ is the determinant of the noise covariance matrix. The joint probability density of K independent samples can be written as

$$p\ (X_1\ X_2, \ldots, X_K \mid \Theta) = \frac{1}{\pi^{NK} \mid R \mid^K} \exp \{ - \sum_{i=1}^{K} \overline{(X_i - bW)}^T\ R^{-1}\ (X_i - bW)\}. \tag{A4}$$

The Cramer-Rao bound on the variance of μ' is obtained from the Fisher's information matrix J whose elements are

$$J_{ij} = E \left\{ \frac{\partial \ln p(X_1, \ldots, X_K \mid \Theta)}{\partial \theta_i} \left[\overline{\frac{\partial \ln p(X_1, \ldots X_K \mid \Theta)}{\partial \theta_j}} \right] \right\}, \tag{A5}$$

where $\theta_1 = \mu'$, $\theta_2 = b$, $\theta_3 = \bar{b}$; E is the expected value operator; and i and j are indices. By using the density function (Eq. (A4)) and the definition (Eq. (A5)), then

$$J_{11} = b\,\bar{b}\left[\frac{\partial \bar{W}}{\partial \mu'} R^{-1} \frac{\partial W}{\partial \mu'} + \frac{\partial W}{\partial \mu'} R^{-1} \frac{\partial \bar{W}}{\partial \mu'}\right] K$$

$$J_{22} = K\,W^T R^{-1}\,\bar{W} = K\,C$$

$$J_{33} = K\,\bar{W}^T R^{-1}\,W = K\,\bar{C}$$

$$J_{12} = b\,K\,\frac{\partial W^T}{\partial \mu'} R^{-1}\bar{w} = b\,K\,A$$

$$J_{13} = \bar{b}\,K\,\frac{\partial \bar{W}^T}{\partial \mu'} R^{-1}W = \bar{b}\,K\,\bar{A}$$

$$J_{21} = \bar{b}\,K\,W^T R^{-1}\,\frac{\partial \bar{W}}{\partial \mu'} = \bar{b}\,K\,\bar{A}$$

$$J_{31} = b\,K\,\bar{W}^T R^{-1}\,\frac{\partial W}{\partial \mu'} = b\,K\,A$$

$$J_{23} = J_{32} = 0.$$

Note that $\frac{\partial W}{\partial \mu'} = BW$ and $\frac{\partial W^T}{\partial \mu'} = W^T B$, where B is defined as the $N \times N$ diagonal matrix:

$$B = \begin{bmatrix} 0 & 0 & \cdot & & 0 \\ 0 & j(2\pi/\lambda)d & \cdot & & \cdot \\ \cdot & \cdot & 2j(2\pi/\lambda)d & & \cdot \\ \cdot & \cdot & \cdot & \cdot & \cdot \\ \cdot & \cdot & \cdot & \cdot & \cdot \\ \cdot & \cdot & \cdot & \cdot & 0 \\ 0 & \cdot & \cdot & & (N-1)j(2\pi/\lambda)d \end{bmatrix}, \qquad \text{(A6)}$$

The matrix J can then be inverted in a closed form

$$J^{-1} = \frac{1}{|J|}\begin{bmatrix} C\bar{C} & -\bar{b}\,A\,\bar{C} & -b\,A\,C \\ -b\,A\,\bar{C} & \bar{C}\,J_{11} - b\,\bar{b}\,A\,\bar{A} & b^2\,A^2 \\ -\bar{b}\,\bar{A}\,C & \bar{b}^2\,\bar{A}^2 & C\,J_{11} - b\,\bar{b}\,A\,\bar{A} \end{bmatrix}^T, \tag{A7}$$

where $|J|$, the determinant of the matrix J, is expressed by

$$|J| = C\,\bar{C}\,J_{11} - b\,\bar{b}\,A\,\bar{A}\,C - b\,\bar{b}\,A\,\bar{A}\,\bar{C}. \tag{A8}$$

The bound on the variance of the estimate of μ' required by the Cramer-Rao bound is

$$\sigma^2_{\mu'} \geq \frac{C\,\bar{C}}{|J|}, \tag{A9}$$

which is the upper left-hand corner of the matrix given in Eq. (A7). Equation (A9) can be explicitly written as

$$\sigma^2_{\mu'} \geq \frac{(W^T R^{-1}\bar{W})(\bar{W}^T R^{-1} W)}{SK[(W^T R^{-1}\bar{W})(\bar{W}^T R^{-1} W)(\bar{W}^T \bar{B} R^{-1} BW + W^T B R^{-1}\bar{B}\bar{W}) - (W^T B R^{-1}\bar{W})(\bar{W}^T \bar{B} R^{-1} W)(W^T R^{-1}\bar{W} + \bar{W}^T R^{-1} W)]}, \tag{A10}$$

where $S = b\bar{b}$ is the signal power.